On the propagation of Voigt waves in energetically active materials

On the propagation of Voigt waves in energetically active materials

2016 Eur. J. Phys. 37 064002

(http://iopscience.iop.org/0143-0807/37/6/064002)

OPEN ACCESS
IOP Publishing
European Journal of Physics
Eur. J. Phys. **37** (2016) 064002 (14pp)
doi:10.1088/0143-0807/37/6/064002

On the propagation of Voigt waves in energetically active materials

Tom G Mackay[1,2,3] **and Akhlesh Lakhtakia**[2]

[1] School of Mathematics and Maxwell Institute for Mathematical Sciences, University of Edinburgh, Edinburgh EH9 3FD, UK
[2] NanoMM—Nanoengineered Metamaterials Group, Department of Engineering Science and Mechanics Pennsylvania State University, University Park, PA 16802–6812, USA

E-mail: T.Mackay@ed.ac.uk and akhlesh@psu.edu

Received 24 May 2016, revised 19 August 2016
Accepted for publication 23 August 2016
Published 22 September 2016

Abstract

If Voigt-wave propagation is possible in a dissipative anisotropic dielectric material characterised by the permittivity dyadic $\underline{\underline{\varepsilon}}$, then it is also possible in the analogous energetically active material characterised by the permittivity dyadic $\underline{\underline{\widetilde{\varepsilon}}}$, where $\underline{\underline{\widetilde{\varepsilon}}}$ is the hermitian conjugate of $\underline{\underline{\varepsilon}}$. This symmetry follows directly from a theoretical analysis of the necessary and sufficient conditions for Voigt-wave propagation in anisotropic materials. As a consequence of this symmetry, a porous dissipative material that exhibits Voigt-wave propagation can be used to construct a material that allows the propagation of Voigt waves with attendant linear gain in amplitude with propagation distance, by means of infiltration with an electrically or optically activated dye, for example. This phenomenon is captured by the Bruggeman formalism for homogenised composite materials based on isotropic dielectric component materials that are randomly distributed as oriented spheroidal particles.

Keywords: Voigt-wave propagation, active materials, anisotropic dielectric materials, homogenised composite materials, Bruggeman formalism

(Some figures may appear in colour only in the online journal)

[3] Author to whom any correspondence should be addressed.

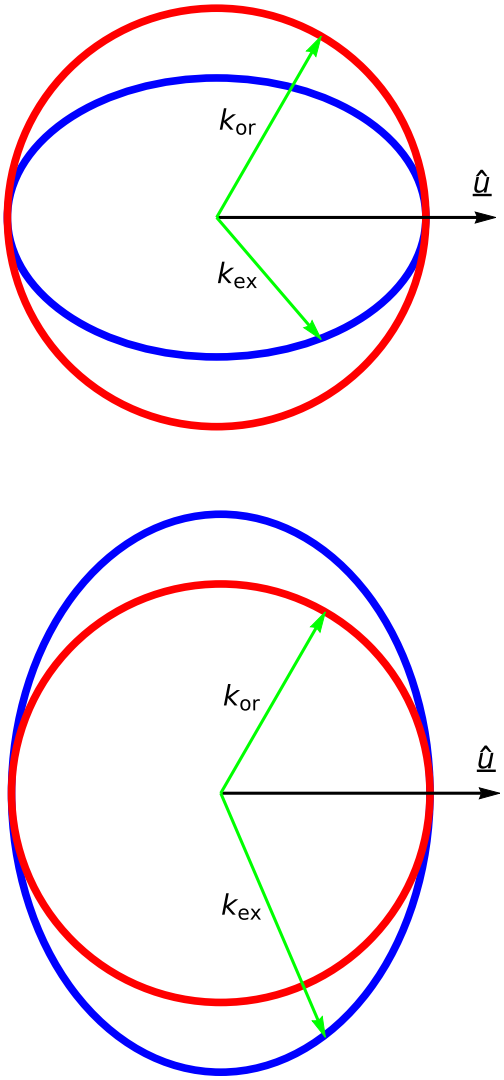

Figure 1. Two-dimensional representations of the surfaces described by the ordinary wavenumber k_{or} (red circles) and the extraordinary wavenumber k_{ex} (blue ellipses) in a nondissipative uniaxial dielectric material characterised by the relative permittivity dyadic $(\underline{I} - \hat{\underline{u}}\,\hat{\underline{u}})\varepsilon_\perp + \hat{\underline{u}}\,\hat{\underline{u}}\,\varepsilon_\parallel$, where $\hat{\underline{u}}$ is aligned with the optic axis while $\varepsilon_{\perp,\parallel} > 0$. The radius of the red circle is $k_0\sqrt{\varepsilon_\perp}$, while the semiaxes of the blue ellipse are of lengths $k_0\sqrt{\varepsilon_\perp}$ and $k_0\sqrt{\varepsilon_\parallel}$. Top: negative uniaxiality (i.e., $\varepsilon_\perp > \varepsilon_\parallel$). Bottom: positive uniaxiality (i.e., $\varepsilon_\perp < \varepsilon_\parallel$).

1. Introduction

Plane-wave analysis is a cornerstone of electromagnetic theory. Although plane waves themselves are idealisations, possessing limitless spatial and temporal extents and limitless energy, they can facilitate deep insights into fields distant from sources; moreover, realistic signals may be conveniently represented as superpositions of plane waves. Therefore,

undergraduate textbooks on electromagnetics and optics invariably present plane waves right after introducing the frequency-domain Maxwell equations and the standard boundary conditions [1–3].

Although many different mathematical techniques can be used to investigate plane-wave propagation either co-parallel or anti-parallel to the unit vector $\hat{\underline{u}}_{\rm prop}$ in a given homogeneous medium, a general method is to substitute $\nabla\times$ by $\mathrm{i}k\hat{\underline{u}}_{\rm prop}\times$ in the frequency-domain Maxwell curl postulates. Here k is the wavenumber, $\imath = \sqrt{-1}$, and an $\exp(-\mathrm{i}\omega t)$ dependence on time t is assumed with ω being the angular frequency. The substitution results in four algebraic equations containing the two components of the electric field and the two components of the magnetic field that are orthogonal to $\hat{\underline{u}}_{\rm prop}$. These four algebraic equations can be written using a 4×4 plane-wave propagation matrix $[P]$ and a column vector containing the four transverse field components [4]. Usually, $[P]$ has four distinct eigenvectors and therefore is diagonalizable [5]. Each eigenvector and the corresponding wavenumber together describe a plane wave. Two of the four plane waves propagate parallel to $\hat{\underline{u}}_{\rm prop}$, while the other two propagate parallel to $-\hat{\underline{u}}_{\rm prop}$. In the remainder of this paper, we consider the two plane waves propagating parallel to $\hat{\underline{u}}_{\rm prop}$, being focused on the situation when the corresponding two eigenvectors are not distinct from each other.

In a nondissipative isotropic dielectric material (as well as in vacuum), both plane waves propagating parallel to $\hat{\underline{u}}_{\rm prop}$ have the same wavenumber but their eigenvectors are distinct (and therefore are mutually orthogonal [5]). As there is only one wavenumber, such a material is called unirefringent. The sole wavenumber does not depend on the direction of propagation. In a nondissipative anisotropic dielectric material, the two plane waves will, in general, have different wavenumbers [6, 7]. Accordingly, such a material is called birefringent. In any uniaxial dielectric material, one of the two plane waves is classified as *ordinary* while the other is classified as *extraordinary*. The wavenumber of the ordinary plane wave does not depend on the direction of propagation, but the wavenumber of the extraordinary plane wave does. Along the two directions aligned with the optic axis of the material, the wavenumbers of the ordinary and the extraordinary plane waves are the same, but their eigenvectors are distinct from each other. The dependences of the wavenumbers of ordinary and extraordinary plane waves are schematically illustrated in figure 1. In a biaxial dielectric material, both plane waves are extraordinary. They have distinct wavenumbers and eigenvectors that depend upon the direction of propagation. There are two optic axes for a biaxial dielectric material, with the wavenumbers of both plane waves being the same for propagation along an optic axis.

A material can be idealized as nondissipative if attenuation of waves can be ignored over the length scales of interest. Matters are further complicated if a material must be considered as dissipative. In certain dissipative anisotropic dielectric materials, there exist directions of propagation—distinct from the directions aligned with the optic axes—along which both plane waves have only one wavenumber and their eigenvectors are not distinct from each other. Both plane waves then coalesce into what is called a Voigt wave [8–12]. A Voigt wave represents a singular form of plane-wave propagation that can arise inside certain dissipative biaxial dielectric materials of the monoclinic and triclinic types [4], as well as inside certain gyrotropic dielectric materials [13, 14], but neither inside nondissipative materials nor inside isotropic or uniaxial dielectric materials.

Mathematically, Voigt-wave propagation arises when the plane-wave propagation matrix $[P]$ cannot be diagonalized [4, 5]. A crucial difference between a Voigt wave and a plane wave propagating along an optic axis is that the amplitude of the Voigt wave varies linearly

with propagation distance whereas this is not the case for the plane wave propagating along the optic axis.

Voigt waves were first investigated experimentally and theoretically for pleochroic crystals [8, 9, 12]. Visible light transmitted through a pleochroic crystal appears to be of different colours when observed from different directions, because the transmission spectrum is direction dependent. Beryl, iolite, and alexandrite are spectacular examples of pleochroic minerals. However, recent research indicates that a greater scope for realizing Voigt-wave propagation is offered by engineered materials [15, 16], especially homogenised composite materials (HCMs) [17, 18]. The directions in which Voigt waves propagate in an HCM may be controlled through careful design of the microstructure and selection of the constitutive properties of the component materials [19], or by the application of an external field in the case of electro-optic materials [20]. Indeed, the ability to control the directions for Voigt-wave propagation is promising for technological applications such as optical sensing [21].

All previous works on Voigt waves have focused on dissipative materials. The issue of Voigt waves in energetically active materials—that is, materials in which plane-wave propagation is accompanied by a net flow of energy from the material to the field—has not been addressed hitherto. The energy that is delivered by an active material may originate externally, from a pump laser, an electrical source, or a radioactive source, for examples. Energetically active materials are useful, or indeed essential, for a host of technoscientific applications. Prime examples are provided by lasing materials, scintillators, and luminescent solar concentrators [22–25]. In this context, let us, for example, single out doped tungstate materials, which can both support Voigt-wave propagation due to their monoclinic crystal symmetry and function as highly efficient lasing materials [26, 27].

The analytical and numerical treatment of Voigt waves involves electromagnetic theory, and a commensurate level of mathematics, accessible to senior undergraduate students of the physical sciences and related engineering disciplines. In particular, the following presentation highlights the usefulness of matrix algebra and complex numbers in physics, and introduces the notion of energetically active materials which is largely conspicuous by its absence in undergraduate electromagnetics courses.

In the following, vectors are denoted by single underlining (with the additional $\hat{}$ symbol indicating a unit vector) while dyadics (i.e., second-rank Cartesian tensors) [7] are denoted by double underlining. The triad of Cartesian basis vectors is $\{\underline{\hat{x}}, \underline{\hat{y}}, \underline{\hat{z}}\}$. The identity dyadic is $\underline{\underline{I}} = \underline{\hat{x}}\,\underline{\hat{x}} + \underline{\hat{y}}\,\underline{\hat{y}} + \underline{\hat{z}}\,\underline{\hat{z}}$, and the null dyadic is $\underline{\underline{0}}$. The permittivity and permeability of free space are $\varepsilon_0 = 8.854 \times 10^{-12}$ F m^{-1} and $\mu_0 = 4\pi \times 10^{-7}$ H m^{-1}, respectively. The operators Re[·] and Im[·] deliver the real and imaginary parts of complex-valued quantities.

2. Symmetry considerations

Let us consider a general anisotropic dielectric material, characterised by the frequency-domain constitutive relations [4]

$$\left.\begin{aligned} \underline{D}(\underline{r}) &= \underline{\underline{\varepsilon}} \bullet \underline{E}(\underline{r}) \\ \underline{B}(\underline{r}) &= \mu_0 \underline{H}(\underline{r}) \end{aligned}\right\}, \tag{1}$$

where the scalars $\varepsilon_{\ell j}$ ($\ell, j \in \{x, y, z\}$) in the permittivity dyadic

$$\begin{aligned} \underline{\underline{\varepsilon}} = \varepsilon_0 (&\varepsilon_{xx}\,\underline{\hat{x}}\,\underline{\hat{x}} + \varepsilon_{xy}\,\underline{\hat{x}}\,\underline{\hat{y}} + \varepsilon_{xz}\,\underline{\hat{x}}\,\underline{\hat{z}} + \varepsilon_{yx}\,\underline{\hat{y}}\,\underline{\hat{x}} + \varepsilon_{yy}\,\underline{\hat{y}}\,\underline{\hat{y}} \\ &+ \varepsilon_{yz}\,\underline{\hat{y}}\,\underline{\hat{z}} + \varepsilon_{zx}\,\underline{\hat{z}}\,\underline{\hat{x}} + \varepsilon_{zy}\,\underline{\hat{z}}\,\underline{\hat{y}} + \varepsilon_{zz}\,\underline{\hat{z}}\,\underline{\hat{z}}) \end{aligned} \tag{2}$$

are complex valued. Without any loss of generality, we focus upon plane-wave propagation along the z axis, i.e., $\hat{\underline{u}}_{\rm prop} = \hat{\underline{z}}$ and $\underline{E}(\underline{r}) = \underline{\tilde{E}}\exp(ikz)$ with $\underline{\tilde{E}} = \tilde{E}_x\,\hat{\underline{x}} + \tilde{E}_y\,\hat{\underline{y}} + \tilde{E}_z\,\hat{\underline{z}}$. The Maxwell curl postulates then yield the 2×2-matrix equation [28]

$$\begin{bmatrix} \delta_{11} & \delta_{12} \\ \delta_{21} & \delta_{22} \end{bmatrix} \begin{bmatrix} \tilde{E}_x \\ \tilde{E}_y \end{bmatrix} = \frac{k^2}{k_0^2}\varepsilon_{zz} \begin{bmatrix} \tilde{E}_x \\ \tilde{E}_y \end{bmatrix}, \tag{3}$$

where $k_0 = \omega\sqrt{\varepsilon_0\mu_0}$ is the free-space wavenumber and the scalar parameters

$$\left.\begin{aligned} \delta_{11} &= \varepsilon_{xx}\varepsilon_{zz} - \varepsilon_{xz}\varepsilon_{zx} \\ \delta_{12} &= \varepsilon_{xy}\varepsilon_{zz} - \varepsilon_{xz}\varepsilon_{zy} \\ \delta_{21} &= \varepsilon_{yx}\varepsilon_{zz} - \varepsilon_{yz}\varepsilon_{zx} \\ \delta_{22} &= \varepsilon_{yy}\varepsilon_{zz} - \varepsilon_{yz}\varepsilon_{zy} \end{aligned}\right\}. \tag{4}$$

Two possible values for the wavenumber k emerge from equation (3), namely

$$k = \begin{cases} k_0\left[\frac{1}{2\varepsilon_{zz}}\{(\delta_{11}+\delta_{22}) + [(\delta_{11}-\delta_{22})^2 + 4\delta_{12}\delta_{21}]^{1/2}\}\right]^{1/2} \\ k_0\left[\frac{1}{2\varepsilon_{zz}}\{(\delta_{11}+\delta_{22}) - [(\delta_{11}-\delta_{22})^2 + 4\delta_{12}\delta_{21}]^{1/2}\}\right]^{1/2} \end{cases}. \tag{5}$$

Usually, in anisotropic dielectric materials these two wavenumbers are distinct from each other, and they are associated with two mutually orthogonal eigenvectors of the 2×2 matrix on the left side of equation (3). However, in the anomalous case of Voigt-wave propagation, these two wavenumbers are identical and the 2×2 matrix on the left side of equation (3) has only one eigenvector. Accordingly, Voigt-wave propagation emerges when the following conditions are satisfied [28]:

(i) $\mathcal{C}_{\rm I}(\underline{\underline{\varepsilon}}) = (\delta_{11} - \delta_{22})^2 + 4\delta_{12}\delta_{21} = 0$, and
(ii) $\mathcal{C}_{\rm II}(\underline{\underline{\varepsilon}}) = \delta_{12} \neq 0$ and/or $\mathcal{C}_{\rm III}(\underline{\underline{\varepsilon}}) = \delta_{21} \neq 0$.

The flow of energy associated with propagation is represented by the time-averaged Poynting vector $\underline{P}(\underline{r}) = (1/2)\mathrm{Re}[\underline{E}(\underline{r}) \times \underline{H}^*(\underline{r})]$, with the superscript * denoting the complex conjugate. In particular, the divergence of the time-averaged Poynting vector is given by [7]

$$\underline{\nabla} \bullet \underline{P}(\underline{r}) = \mathrm{Re}\left\{ \frac{i\omega}{2}[\,\underline{H}^*(\underline{r}) \bullet \underline{B}(\underline{r}) - \underline{E}(\underline{r}) \bullet \underline{D}^*(\underline{r})\,] \right\}. \tag{6}$$

For the anisotropic dielectric material characterised by the constitutive relations (1), the right side of equation (6) simplifies to [7]

$$\underline{\nabla} \bullet \underline{P}(\underline{r}) = \frac{i\omega}{4}\,\underline{E}^*(\underline{r}) \bullet (\underline{\underline{\varepsilon}} - \underline{\underline{\tilde{\varepsilon}}}) \bullet \underline{E}(\underline{r}), \tag{7}$$

where $\underline{\underline{\tilde{\varepsilon}}}$ is the hermitian conjugate of $\underline{\underline{\varepsilon}}$; i.e., the components of $\underline{\underline{\tilde{\varepsilon}}}/\varepsilon_0$ are $\tilde{\varepsilon}_{\ell j} = \varepsilon_{j\ell}^*$ ($\ell \in \{x, y, z\}$ and $j \in \{x, y, z\}$).

Now, if the material characterised by the constitutive relations (1) is:

- dissipative then $\underline{\nabla} \bullet \underline{P}(\underline{r}) < 0$, which, according to equation (7), implies that the three eigenvalues of the dyadic $\underline{\underline{\Psi}} = i(\underline{\underline{\varepsilon}} - \underline{\underline{\tilde{\varepsilon}}})$ are negative valued (i.e., the dyadic $\underline{\underline{\Psi}}$ is negative definite) [5];
- energetically active then $\underline{\nabla} \bullet \underline{P}(\underline{r}) > 0$, which, according to equation (7), implies that the three eigenvalues of $\underline{\underline{\Psi}}$ are positive valued (i.e., $\underline{\underline{\Psi}}$ is positive definite) [5].Therefore, if the

material possessing the permittivity dyadic $\underline{\underline{\varepsilon}}$ is dissipative then the material described by the permittivity dyadic $\underline{\underline{\tilde{\varepsilon}}}$ is energetically active, and vice versa.

Let us turn to the conditions (i) and (ii) that must be satisfied for Voigt-wave propagation. After some algebraic manipulations, one finds

$$\left.\begin{array}{l} \mathcal{C}_{\mathrm{I}}(\underline{\underline{\tilde{\varepsilon}}}) = \mathcal{C}_{\mathrm{I}}^{*}(\underline{\underline{\varepsilon}}) \\ \mathcal{C}_{\mathrm{II}}(\underline{\underline{\tilde{\varepsilon}}}) = \mathcal{C}_{\mathrm{III}}^{*}(\underline{\underline{\varepsilon}}) \\ \mathcal{C}_{\mathrm{III}}(\underline{\underline{\tilde{\varepsilon}}}) = \mathcal{C}_{\mathrm{II}}^{*}(\underline{\underline{\varepsilon}}) \end{array}\right\}. \tag{8}$$

Therefore, if a dissipative (or energetically active) material described by the permittivity dyadic $\underline{\underline{\varepsilon}}$ supports Voigt-wave propagation then so too must the analogous energetically active (or dissipative) material described by the permittivity dyadic $\underline{\underline{\tilde{\varepsilon}}}$.

3. Numerical studies

The Voigt-wave symmetry established in section 2 can be demonstrated, numerically through a consideration of HCMs that permit Voigt waves to propagate, as follows.

3.1. Homogenisation basics

For simplicity, let us consider an HCM comprising just two component materials, one labelled a and the other b. Each component material is taken to be an isotropic dielectric material: the permittivity dyadics $\underline{\underline{\varepsilon}}_a = \varepsilon_0 \varepsilon_a \underline{\underline{I}}$ and $\underline{\underline{\varepsilon}}_b = \varepsilon_0 \varepsilon_b \underline{\underline{I}}$ characterize the electromagnetic properties of the two component materials. The volume fraction of material a is $f_a \in (0, 1)$; correspondingly, the volume fraction of material b is $f_b = 1 - f_a \in (0, 1)$.

Let us imagine that each component material is randomly distributed as spheroidal particles. All particles of material a have the same orientation and all particles of material b have the same orientation, but the orientations of the particles of the different component materials are different. For simplicity, let all particles of both component materials have the same shape, as described by the dyadic

$$\underline{\underline{U}} = U\, \underline{\hat{x}}\, \underline{\hat{x}} + \frac{1}{\sqrt{U}} \left(\underline{\hat{y}}\, \underline{\hat{y}} + \underline{\hat{z}}\, \underline{\hat{z}} \right). \tag{9}$$

The shape parameter $U \in (1, \infty)$ for prolate spheroidal particles, $U = 1$ for spherical particles, and $U \in (0, 1)$ for oblate spheroidal particles.

The position vector

$$\underline{r}_\ell = \eta_\ell\, \underline{\underline{U}}_\ell \bullet \underline{\hat{q}}, \qquad (\ell = a, b) \tag{10}$$

prescribes the surface of every component particle relative to its centroid. On the right side of equation (10), $\underline{\hat{q}}$ is the radial vector that prescribes the surface of the unit sphere, the real symmetric dyadic [7] $\underline{\underline{U}}_\ell$ maps the spherical surface into a spheroidal one, and $\eta_\ell > 0$ is a linear measure of particle size. As the process of homogenisation requires that the component particles be electrically small, let us adopt the standard practice by restricting attention to the limiting regime $\eta_\ell \to 0$. Parenthetically, the typically small effects on Voigt wave propagation that may be introduced by considering the regime wherein η_ℓ is small but not vanishingly small are analytically tractable [19] but lie outside the scope of this paper.

Suppose that the axis of rotational symmetry for the spheroidal particles of material a lies in the xy plane at an angle φ to the x axis; i.e.

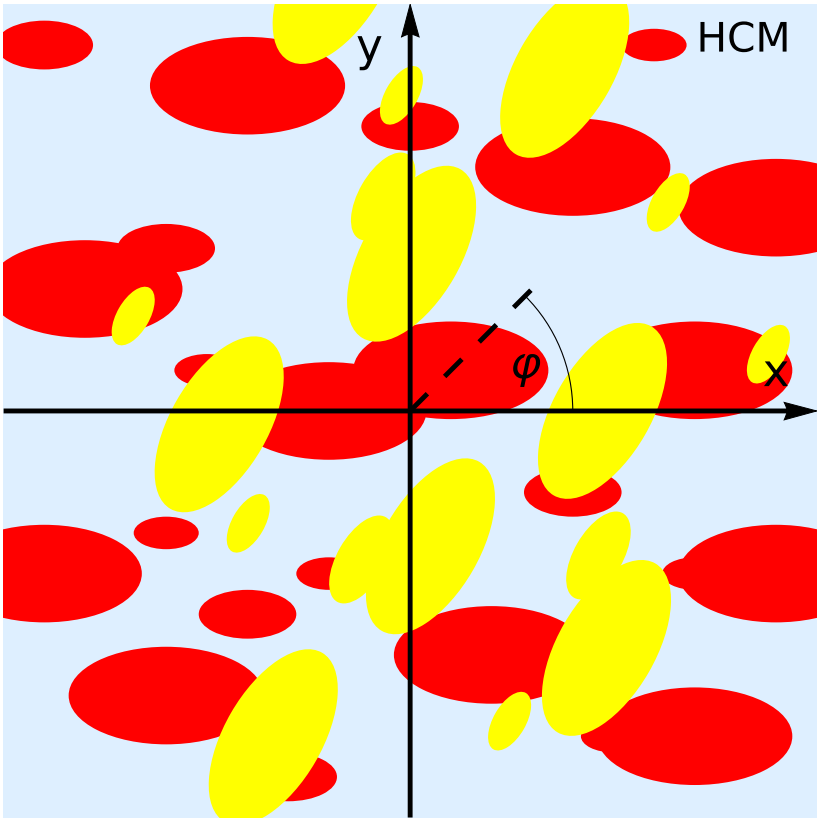

Figure 2. A two-dimensional representation of the two component materials, randomly dispersed as oriented spheroidal particles. Particles of material a (yellow) are oriented at angle φ relative to the particles of material b particles (red). In the Bruggeman formalism, the component particles are supposed to be dispersed inside the HCM (blue).

$$\underline{\underline{U}}_{a} = \underline{\underline{R}}_{z}(\varphi) \bullet \underline{\underline{U}} \bullet \underline{\underline{R}}_{z}^{\mathrm{T}}(\varphi), \tag{11}$$

where the superscript 'T' denotes the transpose operation and the orthogonal rotation dyadic

$$\underline{\underline{R}}_{z}(\varphi) = (\,\underline{\hat{x}}\,\underline{\hat{x}} + \underline{\hat{y}}\,\underline{\hat{y}}\,)\cos\varphi + (\,\underline{\hat{x}}\,\underline{\hat{y}} - \underline{\hat{y}}\,\underline{\hat{x}}\,)\sin\varphi + \underline{\hat{z}}\,\underline{\hat{z}}. \tag{12}$$

Without loss of generality, the axis of rotational symmetry for the spheroidal particles of material b is aligned with the x axis; i.e.

$$\underline{\underline{U}}_{b} = \underline{\underline{U}}. \tag{13}$$

A schematic representation of the two component materials, randomly distributed as oriented spheroidal particles, is provided in figure 2.

Since the orientations of the particles of the two component materials are different from each other, the HCM is a biaxial dielectric material specified by the permittivity dyadic

$$\underline{\underline{\varepsilon}}_{\mathrm{HCM}} = \varepsilon_0\,[\varepsilon_x\,\underline{\hat{x}}\,\underline{\hat{x}} + \varepsilon_y\underline{\hat{y}}\,\underline{\hat{y}} + \varepsilon_t(\underline{\hat{x}}\,\underline{\hat{y}} + \underline{\hat{y}}\,\underline{\hat{x}}\,) + \varepsilon_z\underline{\hat{z}}\,\underline{\hat{z}}]. \tag{14}$$

which is symmetric. In order to estimate $\underline{\underline{\varepsilon}}_{\mathrm{HCM}}$, the Bruggeman homogenisation formalism is implemented. This well-established formalism treats both component materials on an equal footing [29]. Neither component material acts as a host material for the other component

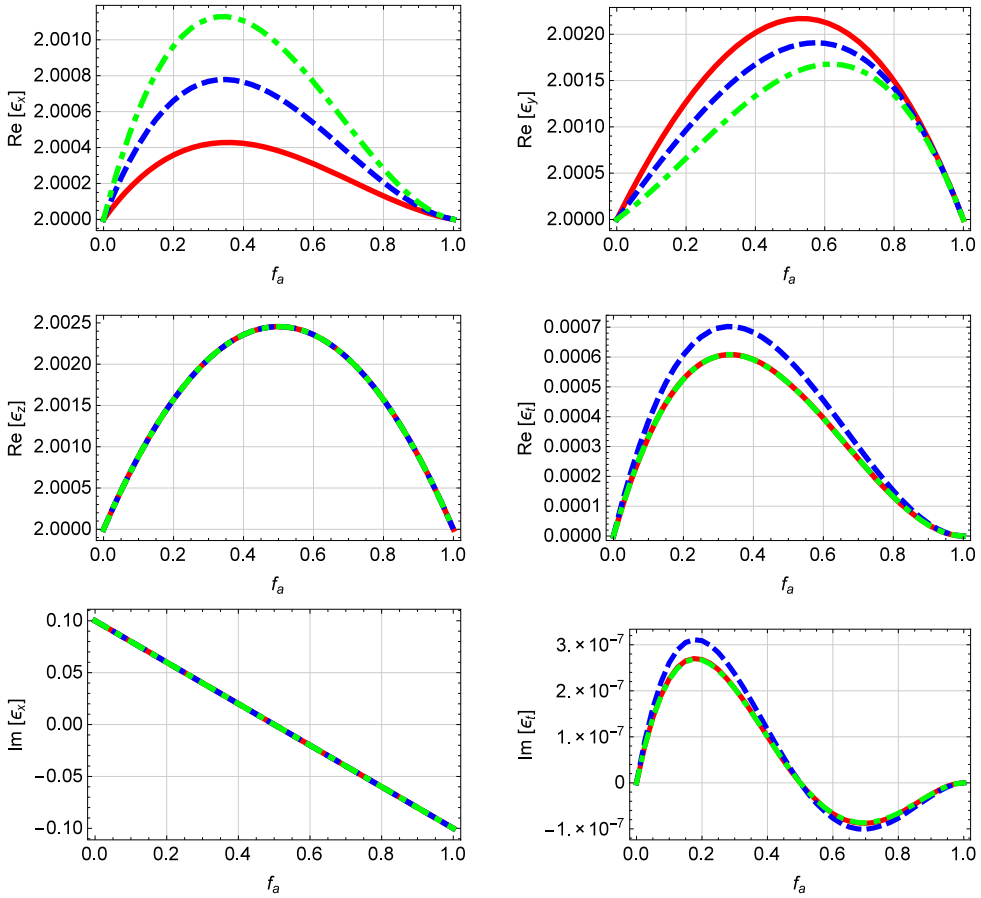

Figure 3. The real and imaginary parts of the HCM's relative permittivity scalars plotted against volume fraction f_a for $\varphi = 30^\circ$ (red, solid curves), 45° (blue, dashed curves), and 60° (green, broken dashed curves), when $\varepsilon_a = 2 - 0.1i$, $\varepsilon_b = 2 + 0.1i$, and $U = 5$. The graphs of $\mathrm{Im}[\varepsilon_y]$ and $\mathrm{Im}[\varepsilon_z]$ are not plotted as they are almost identical to the graph of $\mathrm{Im}[\varepsilon_x]$.

material. On the contrary, the particles of both component materials are taken as dispersed in the HCM itself [30], as indicated in figure 2. As a consequence of this symmetric approach, the Bruggeman formalism may be used for arbitrary values of the volume fractions.

Thereby, $\underline{\underline{\varepsilon}}_{\mathrm{HCM}}$ is extracted from the nonlinear dyadic equation

$$f_a \left\{ (\underline{\underline{\varepsilon}}_a - \underline{\underline{\varepsilon}}_{\mathrm{HCM}}) \bullet [\underline{\underline{I}} + \underline{\underline{D}}_a \bullet (\underline{\underline{\varepsilon}}_a - \underline{\underline{\varepsilon}}_{\mathrm{HCM}})]^{-1} \right\} + f_b \left\{ (\underline{\underline{\varepsilon}}_b - \underline{\underline{\varepsilon}}_{\mathrm{HCM}}) \bullet [\underline{\underline{I}} + \underline{\underline{D}}_b \bullet (\underline{\underline{\varepsilon}}_b - \underline{\underline{\varepsilon}}_{\mathrm{HCM}})]^{-1} \right\} = \underline{\underline{0}}, \tag{15}$$

using standard numerical techniques such as the Jacobi method [31]. The depolarisation dyadics $\underline{\underline{D}}_{a,b}$ on the left side of equation (15) are formulated as the integrals [32, 33]

$$\underline{\underline{D}}_\ell = \frac{1}{4\pi} \iint_{\mathcal{S}} \frac{(\underline{\underline{U}}_\ell^{-1} \bullet \underline{\hat{q}})\,(\underline{\underline{U}}_\ell^{-1} \bullet \underline{\hat{q}})}{(\underline{\underline{U}}_\ell^{-1} \bullet \underline{\hat{q}}) \bullet \underline{\underline{\varepsilon}}_{\mathrm{HCM}} \bullet (\underline{\underline{U}}_\ell^{-1} \bullet \underline{\hat{q}})} \, \mathrm{d}S, \qquad (\ell = a, b), \tag{16}$$

on the surface $\mathcal{S}$ of the unit sphere.

3.2. Voigt-wave propagation in the HCM

Let us now explore Voigt-wave propagation in the HCM formulated in section 3.1 for all possible propagation directions. It is convenient to do so indirectly, by exploring Voigt-wave propagation along the z axis for all possible HCM orientations. Accordingly, the HCM permittivity dyadic is considered in a rotated coordinate system per

$$\underline{\underline{\varepsilon}}^{\dagger}_{\rm HCM}(\alpha,\,\beta,\,\gamma) = \underline{\underline{R}}_z(\gamma) \bullet \underline{\underline{R}}_y(\beta) \bullet \underline{\underline{R}}_z(\alpha) \bullet \underline{\underline{\varepsilon}}_{\rm HCM} \bullet \underline{\underline{R}}^{\rm T}_z(\alpha) \bullet \underline{\underline{R}}^{\rm T}_y(\beta) \bullet \underline{\underline{R}}^{\rm T}_z(\gamma), \tag{17}$$

wherein the orthogonal rotation dyadic

$$\underline{\underline{R}}_y(\beta) = (\,\underline{\hat{x}}\,\underline{\hat{x}} + \underline{\hat{z}}\,\underline{\hat{z}}\,)\cos\beta + (\,\underline{\hat{z}}\,\underline{\hat{x}} - \underline{\hat{x}}\,\underline{\hat{z}}\,)\sin\beta + \underline{\hat{y}}\,\underline{\hat{y}}, \tag{18}$$

and α, β, and γ are the three Euler angles required to obtain the rotated coordinate system [34].

Since propagation parallel to the z axis (of the rotated coordinate system) is independent of rotation about that axis, the angle γ need not be considered henceforth. Furthermore, since $\underline{\underline{\varepsilon}}^{\dagger}_{\rm HCM}$ is symmetric, the conditions $(8)_2$ and $(8)_3$ are identical. Hence, the angles α and β are sought for which the Voigt-wave conditions $\mathcal{C}_{\rm I}(\underline{\underline{\varepsilon}}^{\dagger}_{\rm HCM}) = 0$ and $\mathcal{C}_{\rm II}(\underline{\underline{\varepsilon}}^{\dagger}_{\rm HCM}) \neq 0$ are satisfied.

3.3. An illustrative example

Suppose that the component material a is an energetically active material with relative permittivity $\varepsilon_a = 2 - 0.1i$. This value of ε_a sits within the range commonly used for laser-excited active materials used in metamaterials engineered for the optical regime. For example, across the frequency range 440–500 THz, a mixture of the dyes Rhodamine 800 and Rhodamine 6G (which are two widely used amplification materials) exhibits a relative permittivity with real part in the range (1.8, 2.3) and imaginary part in the range $(-0.15,\,-0.02)$, with the actual values determined by the relative concentrations and the external pumping rate [35]. Accordingly, component material a may be regarded as mixture of these dyes. Component material b is chosen to be a dissipative material with relative permittivity $\varepsilon_b = 2 + 0.1i$. The shape parameter is fixed at $U = 5$.

The Bruggeman estimates of the HCM's relative permittivity scalars $\varepsilon_{x,y,z,t}$ are plotted as functions of the volume fraction f_a in figure 3 for $\varphi \in \{30^\circ,\,45^\circ,\,60^\circ\}$. The dependency upon f_a is such that (i) $\underline{\underline{\varepsilon}}_{\rm HCM} \to \underline{\underline{\varepsilon}}_b$ in the limit $f_a \to 0$ and (ii) $\underline{\underline{\varepsilon}}_{\rm HCM} \to \underline{\underline{\varepsilon}}_a$ in the limit $f_a \to 1$. These two limiting cases correspond to physical reality: particles of material b alone are present when $f_a = 0$, whereas particles of material a alone are present when $f_a = 1$.

The real part of any of the relative permittivity scalars $\varepsilon_{x,y,z,t}$ increases uniformly in figure 3 as f_a increases from 0, reaches a maximum value, and then decreases uniformly as f_a approaches 1, regardless of the value of φ. The graphs of the real parts of $\varepsilon_{x,y,t}$ are slightly asymmetric with respect to reflection in the line $f_a = 0.5$, whereas the graph of ε_z appears to be symmetric in this regard. Also, the graph of the real part of ε_z is independent of the spheroidal orientation in the xy plane (as gauged by the angle φ), which is in contrast to the graphs of the real parts of $\varepsilon_{x,y,t}$. The imaginary part of ε_x decreases in a linear fashion as f_a increases from 0 to 1. Values of $\mathrm{Im}[\varepsilon_x]$ for the three values of φ considered differ by no more than 0.007%. Furthermore, as the corresponding graphs of the imaginary parts of $\mathrm{Im}[\varepsilon_y]$ and $\mathrm{Im}[\varepsilon_z]$ are almost identical to the graphs of $\mathrm{Im}[\varepsilon_x]$, there is no need to display the graphs of $\mathrm{Im}[\varepsilon_y]$ and $\mathrm{Im}[\varepsilon_z]$ here. The graph of $\mathrm{Im}[\varepsilon_t]$ with respect to f_a has a sinusoidal shape with $\mathrm{Im}[\varepsilon_t] > 0$ for $f_a \lessapprox 0.5$ and $\mathrm{Im}[\varepsilon_t] < 0$ for $f_a \gtrapprox 0.5$. The magnitude of $\mathrm{Re}[\varepsilon_t]$ is much smaller than the corresponding magnitudes of the real parts of $\varepsilon_{x,y,z}$; similarly, the magnitude of $\mathrm{Im}[\varepsilon_t]$ is much smaller than the corresponding magnitudes of the imaginary parts of $\varepsilon_{x,y,z}$.

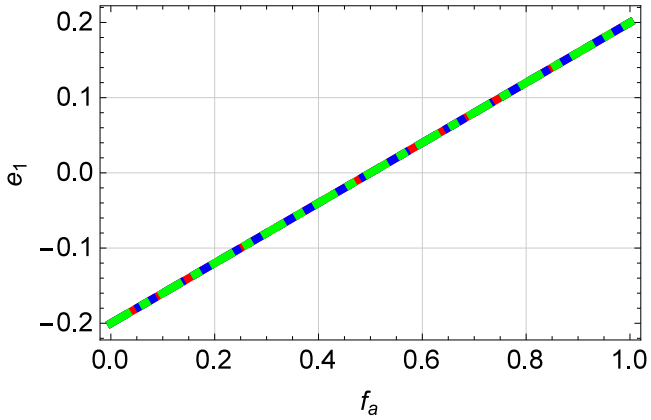

Figure 4. The largest eigenvalue e_1 of the real symmetric dyadic $\underline{\underline{\Psi}}_{\rm HCM}$ plotted against volume fraction f_a, for $\varphi = 30^\circ$ (red, solid curves), 45° (blue, dashed curves), and 60° (green, broken dashed curves), when $\varepsilon_a = 2 - 0.1i$, $\varepsilon_b = 2 + 0.1i$, and $U = 5$.

For which values of f_a is the HCM an energetically active material and for which values of f_a is the HCM a dissipative material? To answer this question, the three eigenvalues of the real symmetric dyadic $\underline{\underline{\Psi}}_{\rm HCM} = {\rm i}(\underline{\underline{\varepsilon}}_{\rm HCM} - \underline{\underline{\tilde{\varepsilon}}}_{\rm HCM})$ must be considered. Let us denote these three eigenvalues by e_1, e_2, and e_3, with $e_1 \geqslant e_2 \geqslant e_3$.

The eigenvalue e_1 is plotted in figure 4 against the volume fraction f_a for $\varphi \in \{30^\circ, 45^\circ, 60^\circ\}$. The value of e_1 increases in a linear fashion from -0.2 at $f_a = 0$ to 0.2 at $f_a = 1$. Values of e_1 for the three values of φ differ by no more than 0.007%. Furthermore, there is no need to display here the corresponding graphs for e_2 and e_3 since these are very similar to those for e_1 in figure 4. Although the values of $e_{1,2,3}$ are not exactly the same, they are very close because the degree of anisotropy exhibited by the HCM here is rather modest.

From figure 4, we infer that the HCM is a dissipative material for $f_a \lessapprox 0.5$ and an energetically active material for $f_a \gtrapprox 0.5$. Parenthetically, there exists a tiny range of the volume fraction f_a, centred at $f_a = 0.5$, for which the three eigenvalues $e_{1,2,3}$ do not all have the same sign and hence the dyadic $\underline{\underline{\Psi}}_{\rm HCM}$ is neither positive definite nor negative definite, but is indefinite instead. In this tiny range of f_a, the HCM can simultaneously amplify electromagnetic signals for certain propagation directions and attenuate electromagnetic signals for other propagation directions [36]. However, for the example considered here, this volume fraction range is so small that we need not consider this matter further.

Now we turn to Voigt-wave propagation in the HCM characterised in figures 3 and 4. In general, at fixed values of f_a and φ, the Voigt-wave conditions $\mathcal{C}_{\rm I}(\underline{\underline{\varepsilon}}^{\,\dagger}_{\rm HCM}) = 0$ and $\mathcal{C}_{\rm II}(\underline{\underline{\varepsilon}}^{\,\dagger}_{\rm HCM}) \neq 0$ are satisfied for two distinct orientations, as specified by the angle pairs $\{\alpha_1, \beta_1\}$ and $\{\alpha_2, \beta_2\}$. In figure 5, α_1, β_1, and the corresponding value of the quantity $|\mathcal{C}_{\rm II}(\underline{\underline{\varepsilon}}^{\,\dagger}_{\rm HCM})|$ are plotted against f_a for $\varphi \in \{30^\circ, 45^\circ, 60^\circ\}$. The angle α_1 increases uniformly as f_a increases from 0 to 1, for all values of φ considered. On the other hand, the angle β_1 decreases uniformly as f_a increases from 0, reaches a minimum at $f_a = 0.5$, and then increases uniformly as f_a increases to 1, for all values of φ considered. The quantity $|\mathcal{C}_{\rm II}(\underline{\underline{\varepsilon}}^{\,\dagger}_{\rm HCM})| \neq 0$ for $0 < f_a \lessapprox 0.5$ and for $0.5 \lessapprox f_a < 1$. However, $|\mathcal{C}_{\rm II}(\underline{\underline{\varepsilon}}^{\,\dagger}_{\rm HCM})| \approx 0$ at $f_a \approx 0.5$. Thus, Voigt-wave propagation is not possible when the HCM is neither energetically active nor dissipative, i.e., when $\underline{\underline{\varepsilon}}_{\rm HCM}$ is real valued.

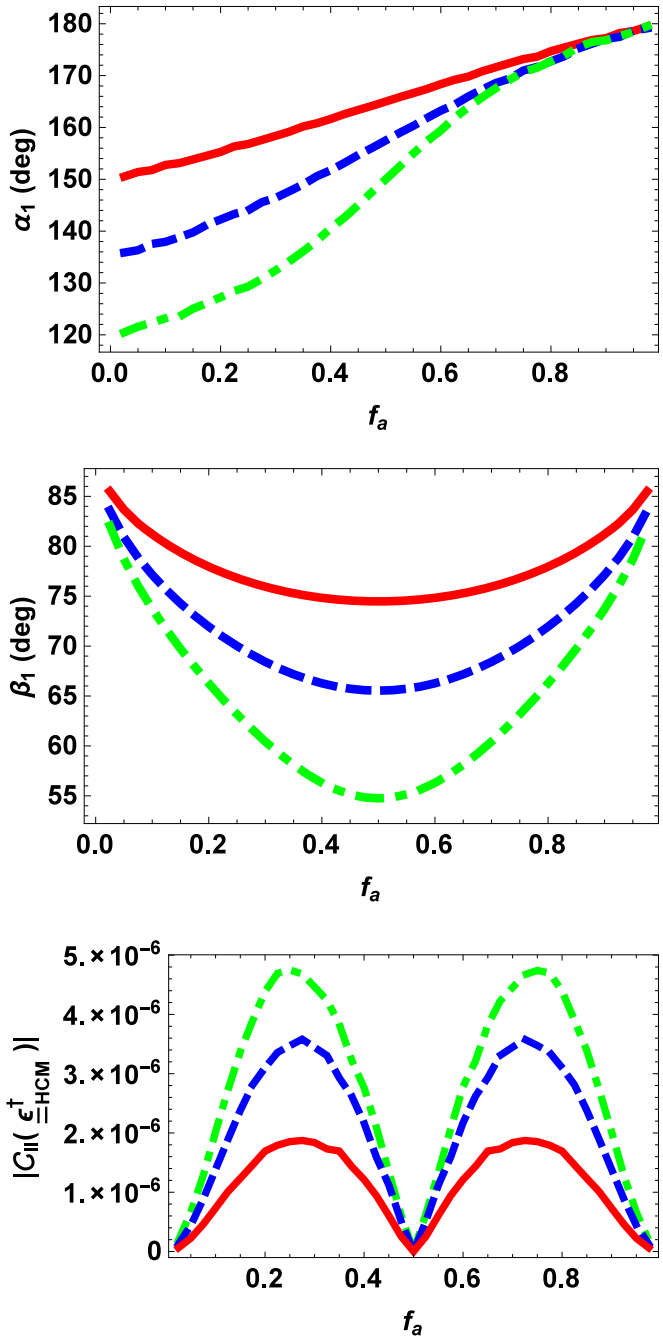

Figure 5. The angles α_1 and β_1, and the corresponding quantity $|\mathcal{C}_{\rm II}(\underline{\underline{\varepsilon}}^{\dagger}_{\rm HCM})|$, plotted against volume fraction f_a, for $\varphi = 30^\circ$ (red, solid curves), 45° (blue, dashed curves), and 60° (green, broken dashed curves), when $\varepsilon_a = 2 - 0.1i$, $\varepsilon_b = 2 + 0.1i$, and $U = 5$.

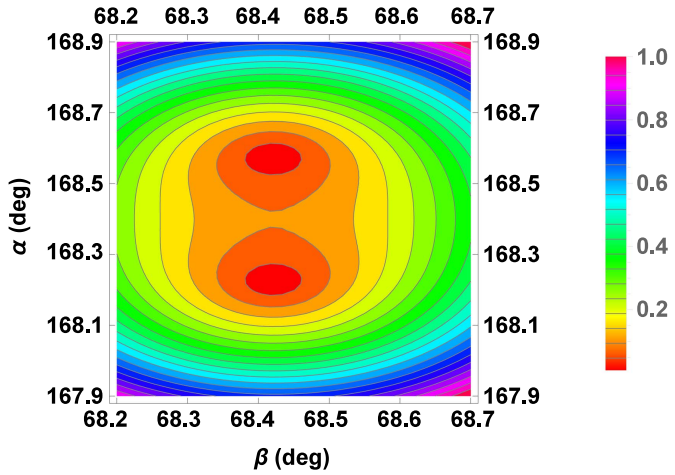

Figure 6. The normalised value of $|\mathcal{C}_{\rm I}(\underline{\underline{\varepsilon}}^{\dagger}_{\rm HCM})|$ mapped as a function of the angles $\alpha \in (167.9^\circ, 168.9^\circ)$ and $\beta \in (68.2^\circ, 68.7^\circ)$ for $f_a = 0.7$ and $\varphi = 45^\circ$, when $\varepsilon_a = 2 - 0.1i$, $\varepsilon_b = 2 + 0.1i$, and $U = 5$.

The analogous plots of the angles α_2 and β_2 are very similar to those of α_1 and β_1 provided in figure 5. Indeed, our numerical investigations revealed that the differences between α_1 and α_2, and between β_1 and β_2, were less than 1% (and often much smaller). A representative illustration of the closeness of the two distinct directions for Voigt-wave propagation is presented in figure 6. Therein, the normalised values of the quantity $|\mathcal{C}_{\rm I}(\underline{\underline{\varepsilon}}^{\dagger}_{\rm HCM})|$ are depicted for $\alpha \in (167.9^\circ, 168.9^\circ)$ and $\beta \in (68.2^\circ, 68.7^\circ)$, when $f_a = 0.7$ and $\varphi = 45^\circ$. For this example, the zeros of $|\mathcal{C}_{\rm I}(\underline{\underline{\varepsilon}}^{\dagger}_{\rm HCM})|$ occur at $(\alpha, \beta) = (168.23^\circ, 68.42^\circ)$ and $(\alpha, \beta) = (168.57^\circ, 68.42^\circ)$. Greater differences between the two orientations for Voigt-wave propagation emerge for HCMs that exhibit greater degrees of anisotropy—as may be achieved when one (or more) of the component materials is itself anisotropic, for example [17].

4. Closing remarks

An important implication of this study is as follows. Suppose we consider a certain dissipative material, say a porous composite material that should have monoclinic symmetry according to homogenisation formalisms. Voigt waves can propagate in this composite material with attendant linear attenuation as the propagation distance increases [17]. Now if this composite material were to be infiltrated with a sufficient quantity of an energetically active dye (which is fluorescent [37]), such that the monoclinic symmetry remained unchanged, then Voigt waves *could* propagate in this material with attendant linear gain as the propagation distance increased. Thus, the usual exponential amplification of power density with distance (that will occur in every direction and will depend on birefringence) will be enhanced by linear amplification with distance only along the directions that allow Voigt-wave propagation. This highly directional amplification could be exploited, for example, to enhance visible light communication for extremely rapid uploading and downloading of information [38, 39].

Acknowledgments

TGM acknowledges the support of EPSRC grant EP/M018075/1. AL thanks the Charles Godfrey Binder Endowment at Penn State for ongoing support of his research activities.

References

[1] Hayt W H Jr and Buck J A 2011 *Engineering Electromagnetics* 8th edn (New York: McGraw-Hill)
[2] Iskander M F 2012 *Electromagnetic Fields and Waves* 2nd edn (Long Grove, IL: Waveland)
[3] Ida N 2015 *Engineering Electromagnetics* 3rd edn (New York: Springer)
[4] Mackay T G and Lakhtakia A 2008 Electromagnetic fields in linear bianisotropic mediums *Prog. Opt.* **51** 121–209
[5] Whitelaw T A 1995 *Introduction to Abstract Algebra* 3rd edn (Glasgow: Blackie)
[6] Born M and Wolf E 1980 *Principles of Optics* 6th edn (Oxford: Pergamon)
[7] Chen H C 1983 *Theory of Electromagnetic Waves* (New York: McGraw-Hill)
[8] Voigt W 1902 On the behaviour of pleochroitic crystals along directions in the neighbourhood of an optic axis *Phil. Mag.* **4** 90–7
[9] Pancharatnam S 1955 The propagation of light in absorbing biaxial crystals:I. Theoretical *Proc. Ind. Acad. Sci.* A **42** 86–109
[10] Khapalyuk A P 1962 On the theory of circular optical axes *Opt. Spectrosc.* **12** 52–4
[11] Fedorov F I and Goncharenko A M 1963 Propagation of light along the circular optical axes of absorbing crystals *Opt. Spectrosc.* **14** 51–3
[12] Ranganath G S 1994 Optics of absorbing anisotropic media *Curr. Sci.* **67** 231–7
[13] Agranovich V M and Ginzburg V L 1984 *Crystal Optics with Spatial Dispersion, and Excitons* (Berlin: Springer)
[14] Grechushnikov B N and Konstantinova A F 1988 Crystal optics of absorbing and gyrotropic media *Comput. Math. Appl.* **16** 637–55
[15] Lakhtakia A 1998 Anomalous axial propagation in helicoidal bianisotropic media *Opt. Commun.* **157** 193–201
[16] Berry M V 2005 The optical singularities of bianisotropic crystals *Proc. R. Soc.* A **461** 2071–98
[17] Mackay T G and Lakhtakia A 2003 Voigt wave propagation in biaxial composite materials *J. Opt. A: Pure Appl. Opt.* **5** 91–5
[18] Mackay T G and Lakhtakia A 2004 Correlation length facilitates Voigt wave propagation *Waves Random Media* **14** L1–11
[19] Mackay T G 2011 Voigt waves in homogenized particulate composites based on isotropic dielectric components *J. Opt.* **13** 105702
[20] Mackay T G 2015 Controlling Voigt waves by the Pockels effect *J. Nanophoton* **9** 093599
[21] Mackay T G 2014 On the sensitivity of directions that support Voigt wave propagation in infiltrated biaxial dielectric materials *J. Nanophoton* **8** 083993
[22] Hecht J 2008 *Understanding Lasers: An Entry-Level Guide* 3rd edn (Piscataway, NJ: IEEE)
[23] Vij D K (ed) 1998 *Luminescence of Solids* (New York: Plenum)
[24] Yukihara E G and McKeever S W S 2011 *Optically Stimulated Luminescence: Fundamentals and Applications* (Chicester: Wiley)
[25] Debije M G and Verbunt P P C 2012 Thirty years of luminescent solar concentrator research: solar energy for the built environment *Adv. Energy Mater* **2** 12–35
[26] Kaminskii A A, Ueda K, Eichler H E, Findeisen J, Bagayev S N, Kuznetsov F A, Pavlyuk A A, Boulon G and Bourgeois F 1998 Monoclinic tungstates KDy $(WO_4)_2$ and KLu $(WO_4)_2$-new $\chi^{(3)}$ active crystals for laser Raman shifters *Japan. J. Appl. Phys.* **37** L923–6
[27] Karek A, Boudellioua A, Lebbou K, Brenier A and Boulon G 2009 Structural and spectroscopic characterization of the double tungstate NaBi $(WO_4)_2$ crystals doped with Yb^{3+} and grown by the micro-pulling down technique *Phys. Proc.* **2** 497–500
[28] Gerardin J and Lakhtakia A 2001 Conditions for Voigt wave propagation in linear, homogeneous, dielectric mediums *Optik* **112** 493–5
[29] Mackay T G and Lakhtakia A 2015 *Modern Analytical Electromagnetic Homogenization* (Bristol: IOP Publishing)

[30] Ross B M and Lakhtakia A 2005 Bruggeman approach for isotropic chiral mixtures revisited *Microw. Opt. Technol. Lett.* **44** 524–7
[31] Buchanan J L and Turner P R 1992 *Numerical Methods and Analysis* (New York: McGraw-Hill)
[32] Michel B 1997 A Fourier space approach to the pointwise singularity of an anisotropic dielectric medium *Int. J. Appl. Electromagn. Mech.* **8** 219–27
[33] Michel B and Weiglhofer W S 1997 Pointwise singularity of dyadic Green function in a general bianisotropic medium *Arch. Elekron. Übertrag* **51** 219–23
Michel B and Weiglhofer W S 1998 *Arch. Elekron. Übertrag* **52** 31 (erratum)
[34] Arfken G B and Weber H J 1995 *Mathematical Methods for Physicists* 4th edn (London: Academic)
[35] Sun L, Yang X and Gao J 2013 Loss-compensated broadband epsilon-near-zero metamaterials with gain media *Appl. Phys. Lett.* **103** 201109
[36] Mackay T G and Lakhtakia A 2015 Dynamically controllable anisotropic metamaterials with simultaneous attenuation and amplification *Phys. Rev.* A **92** 053847
[37] Jameson D M 2014 *Introduction to Fluorescence* (Boca Raton, FL: CRC Press)
[38] Haas H 2011 Wireless data from every light bulb http://ted.com/talks/harald_haas_wireless_data_from_every_light_bulb (accessed 23 May 2016)
[39] Arnon S (ed) 2015 *Visible Light Communication* (Cambridge: Cambridge University Press)